OPEN ACCESS INTERNATIONAL JOURNAL OF SCIENCE & ENGINEERING

GREEN MEDIATED SYNTHESIS OF Ce DOPED Cdo NANO CRYSTALS: STUDY OF ITS MAGNETIC AND PHOTOLUMINESCENCE CHARACTERS

M.S.Geetha[1*], H. Nagabhushana[2], H. N. Shivananjaiah[3]
Vijaya Composite College, Bangalore,560 011, India.[1]
CNR Rao centre for Advanced materials, Tumkur University, Tumkur 572 103, India.[2]
Government Science College, Nrupatunga road, Bangalore,560 001, India.[3]
geethashivu33@gmail.com

Abstract: **In this present work, we have doped CdO with Ce and studied its various properties and characters systematically. CdO nano crystals with different Ce concentrations (0.5% to 5%) have been synthesized by combustion method using Aloe vera plant latex as reducing agent. As synthesised product was characterised using powder X-ray diffraction (PXRD) , UV Visible spectroscopy (UV-Vis), Rietveld refinement, scanning electron microscopy with energy dispersion spectroscopy (SEM with EDS),transmission electron microscopy (TEM), Raman spectroscopy, Ferro electric studies, X-ray photoelectron spectroscopy (XPS), anti bacterial and Photo luminescence (PL).The PXRD patterns shows size of the particles 44nm to 28nm. Rietveld refinement of PXRD showed cubical phase of the crystals with a = 4.68A°. XPS is an important tool to study the chemical composition of a compound. Thus Ce doped CdO was characterised by XPS. Comparing the results obtained with the provided standard wide spectra, it was clearly shown the existence of Ce as a doping element in CdO. When we studied optical absorption spectra , the maximum absorption wave length was found to shifted slightly towards shorter wave length (blue shift) when compared with that of pure CdO. The optical energy gap of Ce doped CdO NPs was found to be ~3.05 eV. SEM with EDS and TEM showed particles are spherical in shape with nm size. EDS confirmed the absence of impurities in the crystals. CdO doped with Ce exhibits hysteresis with retentivity 0.01092 emu and cohercivity 0.008939kOe. Its antibacterial properties showed that the compound is effective on Bacillus subtillis (Gram positive) and Staphylococcus (gram positive) bacteria. The emission peaks at 435 nm, 549 nm and 646 nm were due to the transitions of $^5D_3 \rightarrow {}^7F_4$, $^5D_4 \rightarrow {}^7F_5$ and $^5D_4 \rightarrow {}^7F_3$ corresponds to Ce^{3+} ions. The Commission International de I'Eclairage and colour correlated temperature coordinates were estimated for all the concentrations of Ce^{3+} ions and the results indicates that the phosphor may quite useful in cool light source.**

Keywords: Aloe vera latex, SEM with EDS, XPS, M-H plot, Anti bacterial, PL studies.

I INTRODUCTION

Now a day's nano technology is growing very fast, as it involves the manufacture, processing and application of structures, systems and devices by controlling the shape and size at the nano meter scale. Recently, the interest in studying metal oxide semiconductors which are nano structured has increased among researchers because the low dimensionality of the compound results in quantum size effect. This quantum size effect causes unique size and shape dependent physical and chemical properties. In the present scenario researchers are working on synthesis and characterization of transparent conduction oxides (TCO) namely CdO, ZnO, SnO_2, Ga_2O_3, In_2O_3 etc. TCO's have a wide range of applications in electronic technology particularly in optoelectronic and other applications like photodiodes, solar cells, photo transistors, gas sensors and transparent electrodes [1-5]. The chemical synthesis methods called green mediated synthesis are getting lot a of interest because they are safe and ecofriendly. In this scenario, our focus is on development of new material and methods for green mediated synthesis of nano particles.

Due to the interesting properties of CdO such as high transparency, high conductivity and other prominent applications, it has attracted researchers worldwide. CdO is

an extrinsic semiconductor of n-type . It has 2.5 eV as the direct band gap and 2.0 eV as an indirect band gap [6]. Researchers are trying to manipulate the characters by going for a mixture of materials. One of the methods in achieving this, is by doping the semiconductors with transition metals, which are popularly known as dilute magnetic semiconductors. In dilute magnetic semiconductors some of the host cations can be replaced by magnetic ions. These dilute magnetic semiconductors can be used for basic research and various technological applications [7]. They are very well studied that the doping of elements like Aluminum [8], Boron [9] and Barium [10] in semiconducting nanostructures opens the possibilities of building up a new class of materials with novel properties and with lot of technological applications. Dilute magnetic semiconductors are more attractive because of their applications in the field of spintronics [11]. These spintronics devices can be used in spin valves, non- volatile memories, spin light emitting diodes and magnetic sensors. Synthesis of compounds using the elements of second and sixth group, dilute magnetic semiconductors provides a material with both magnetic and semiconducting characters [12]. The wide applications and above discussed studies inspired us to perform systematic studies on Ce doped and undoped CdO nanoparticles.

Benhaliliba et al reported copper doped CdO derived nanostructures. They reported synthesis of Cu doped CdO by Sol-gel method and observed significant increase in the conductivity of the sample with doping [13]. Aswani et al reported the synthesis of Cu^{2+} doped CdO Nano powder solid state reaction method. They reported in PL studies that doped CdO exhibits a strong blue-green emission band at 427, 481 nm[14]. Alahmed et al reported synthesis of Mn doped CdO thin films by sol–gel spin coating method. They reported an average crystallite size of 22–25 nm. S. Kumar et al synthesized Mn doped nano structure and studied the Ferro magnetic nature [15]. Sahin et al synthesized Ba-doped CdO thin films and reported an increase in band gap energy with increase in barium doping concentration [16].Y. Gulen et al. has synthesized lead doped CdO by successive ionic layer adsorption and reaction (SILAR) technique. They reported a PL absorption edge shift towards a shorter wave length due to change in crystallite size [17].Sivakumar et al. synthesized Al doped CdO and studied its antibacterial characters [18].Sivakumar et al synthesized Ba doped CdO nano particles and reported that the particles are active both on gram positive and gram negative bacteria [19].

II RESULTS AND DISCUSSION

2.1. Powder X-ray diffraction (PXRD)

Fig 1(a) shows the PXRD profiles of undoped and doped NPs. Well defined peaks indicate that the NPs were well crystallised. The peaks correspond to (hkl) values (111), (200), (220), (311) and (222) respectively. No other impurity peaks were observed. It is observed that as the doping concentration increases, the peaks slightly shift towards a smaller angle and the intensity of the peaks changes slightly. This is because of the presence of doping element Ce^{3+} in the interstitial positions of CdO [Fig 1(b)].

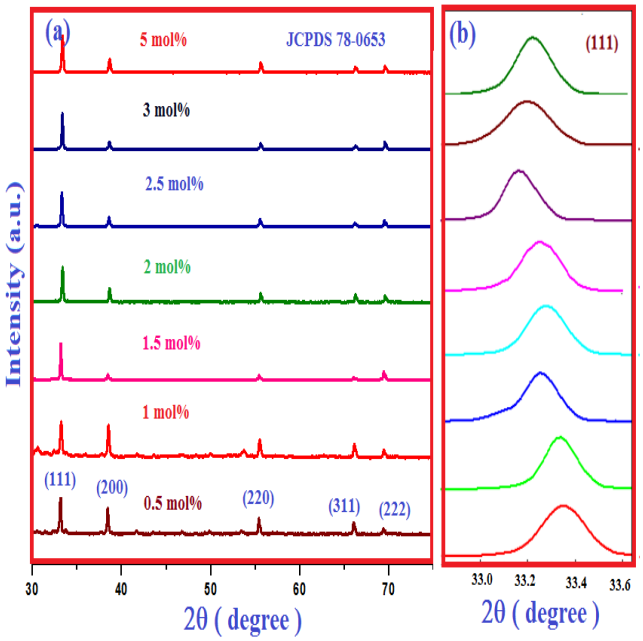

Figure 1 PXRD patterns of Ce doped and undoped CdO prepared using latex of *Aloe vera* as reducing agent

The crystallite size was estimated for the powder from the FWHM (full width half maximum) of the diffraction peaks using Scherrer equation and Williamson Hall modified form Uniform Deformation Model (UDM), Uniform Stress Deformation Model (USDM), Uniform Deformation Energy-Density Model (UDEDM) [21,22].

The crystal size was calculated using Scherrer equation,

$$D = k\lambda / \beta\cos\theta \quad \ldots\ldots\ldots\ldots\ldots\ldots (1)$$

where D is the crystal size, k is the shape constant (~0.9), λ is the X ray wavelength, θ is the Bragg's angle and β is the line broadening at half the maximum intensity (FWHM) in radians. The average crystallite sizes of doped and undoped CdO NPs are given in Table 1. From the above Table it was observed that as the doping concentration increases, the particle size decreases. Even though Aloe vera concentration is same, mass of host $Cd(NO_3)_2$ decreases, where as mass of doping element $Ce(NO_3)_2$ increases. The decrease in crystallite size with increase in fuel/oxidant molar ratio may be due to number of moles of gaseous products liberated.

Table 1 Crystallite size, strain, Dislocation density and stress of Ce doped CdO nano particles prepared by various concentration of Aloe vera latex

Sample	Scherrer equation	Strain	Dislocation density	Stress
	D (nm)	$\epsilon \times 10^{-3}$	$\delta = 1/D^2 \times 10^{15}$	$\sigma = \epsilon Y$ (M Pa)
CdO	44	0.83	0.5165	107.9
CdO: 0.5 mol%	43	0.851	0.5408	110.63
CdO: 1 mol%	41	0.886	0.5948	115.18
CdO:1.5 mol%	40	0.9046	0.625	117.598
CdO:2 mol%	39	0.9266	0.6574	120.458
CdO:2.5 mol%	34	1.027	0.865	133.51
CdO:3 mol%	31	1.115	1.0405	144.95
CdO:5 mol%	28	1.226	1.2755	159.38

As more gases are liberated with the increase in fuel to oxidant molar ratio, the agglomerates disintegrate and additional heat is carried away from the system thereby hindering the particle growth, which in turn produces nanoparticles of smaller size with high specific area . Similar observations have been reported by other researchers. Micro strain is calculated using the equation

$$\varepsilon = \beta \cos\theta / 4 \quad \ldots\ldots\ldots\ldots\ldots\ldots (2)$$

Further the dislocation density(δ) of CdO NPs are calculated by William and Smallman's equation

$$\delta = 1/D^2 \quad \ldots\ldots\ldots\ldots\ldots\ldots (3)$$

where D is the crystal size in nm. As strain and dislocation density are inversely proportional to the particle size, they are found to increase with decrease in the particle size (Table 1). The small dislocation density δ for doped CdO NPs indicates higher crystallisation of the sample. Thus in doped CdO NPs, CdO with 5% doping shows high level of surface defects and deteriorates crystal quality. But 0.5% doped NPs shows the low level of surface defects.

The crystallite size was also estimated for the powder from the FWHM of the diffraction peaks using Williamson Hall modified form. Depending on different angular positions the separation of size and strain broadening analysis was done using Williamson and Hall (WH) plots. The following results are the addition of the Scherrer equation and $\varepsilon \approx \beta s/\tan\theta$. Therefore

$$\beta_{hkl} = (k\lambda/D \cos\theta) + 4\varepsilon \tan\theta \quad \ldots\ldots\ldots\ldots\ldots\ldots (4)$$

Rearranging this equation we get

$$\beta \cos\theta = k\lambda/D + 4\varepsilon \sin\theta \quad \ldots\ldots\ldots\ldots\ldots\ldots (5)$$

This equation stands for UDM, where it is assumed that strain was uniform in all crystallographic directions. The strain observed during lattice parameters calculations might be due to the shrinkage of lattice. Fig 2 (a) shows W-H plot (UDM) of doped CdO NPs using *Aloe vera* latex as fuel.

Using the intercept and slope, particle size and micro strain were calculated. UDM analysis is shown in Table 2. According to Hooke's law stress is directly proportional to strain within the elastic limit. Therefore

$$\sigma = Y\varepsilon \quad \ldots\ldots\ldots\ldots\ldots\ldots (6)$$

Where σ is the stress and Y is the Young's modulus. USDM was a plot of βcosθ versus 4 sinθ /Y (where $Y= 130\times10^9$ Nm^{-2}). The USDM plot is shown in Fig 2 (b)

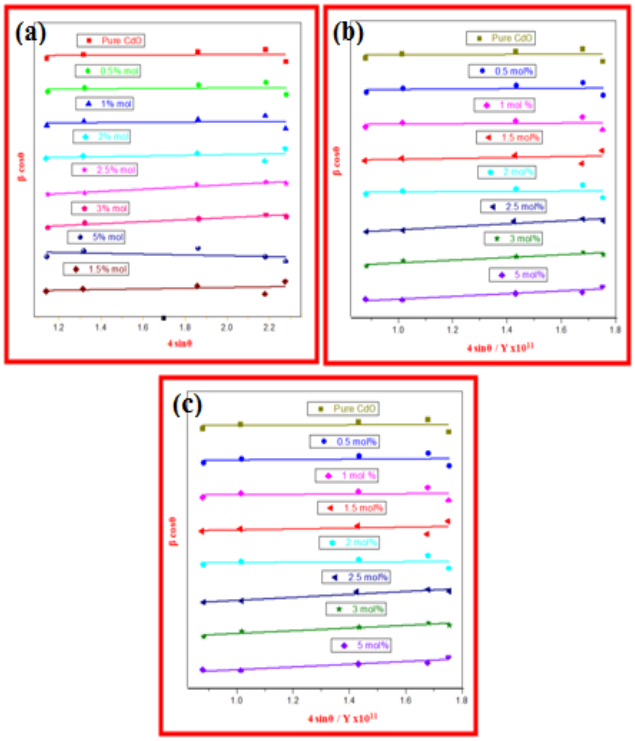

Figure 2 UDM plot, USDM plot and UDEDM plot of Ce doped CdO NPs

Using intercept and slope, particle size and stress were calculated. Then strain $\varepsilon = \sigma/Y$. The results were tabulated in Table 2.The graph of β cosθ versus $4\sin\theta/(Y/2)^{1/2}$ (where $Y= 130\times10^9$ Nm^{-2}) represents UDEDM plot. The plot of βcosθ versus $4 \sin\theta /(Y/2)^{1/2}$ is shown in Fig 2 (c). Using the intercept and slope particle size and energy density were calculated. Micro strain $\varepsilon = (2u / Y)^{1/2}$ and stress $\sigma = \varepsilon Y$ were also calculated. UDEDM analysis results are shown in Table 2. From the table we can conclude that as the particle size decrease, strain increases and energy density increases.

Table 2 Crystallite size, strain, stress and energy density of Ce doped CdO nano particles prepared by various concentration of Aloe vera latex

Ce^{3+} con. mol%	UDM D nm	UDM ϵ $\times 10^{-3}$	USDM D nm	USDM ϵ $\times 10^{-3}$	USDM σ = ϵ Y M Pa	UDEDM D nm	UDEDM ϵ $\times 10^{-3}$	UDEDM σ = ϵ Y M Pa	UDEDM U kJm^{-3}
Pure	46	0.15	46	0.15	20.3	46	0.15	20.3	1.59
0.5	45	0.17	45	0.17	22.9	45	0.17	22.9	2.02
1	43	0.27	43	0.27	35.7	43	0.27	35.7	4.90
1.5	42	0.71	42	0.71	93.0	42	0.71	93.0	33.2
2	40	0.92	40	0.92	120	40	0.92	120	54.9
2.5	35	1.00	35	1.00	131	35	1.00	131	66.1
3	32	1.11	32	1.11	145	32	1.11	145	80.9
5	28	2.07	28	2.07	270	28	2.07	270	280

2.2 SEM with EDS and TEM

SEM images of CdO NPs with different Ce^{3+} concentration are shown in Fig 3. By comparing the micrographs with different doping concentrations, it was evident that doping concentration played a significant role in the morphology of CdO NPs. The undoped CdO NPs exhibit agglomerated particles Fig 3 (a). As the doping concentration increases, agglomeration decreased. At 5 mol% of Ce^{3+} well defined spherical particles of average particle size around 100 nm were obtained, which is also supported by PXRD results. Normally in green mediated synthesis two types of reactions are possible. 1) Interaction of cavitational bubble with the bulk surrounding solution, which leads to well defined crystalline structure and 2) collapse of bubbles inside the bulk solution leads to amorphous material. Here, well defined particles signify the interaction of the bubbles with the bulk solution.

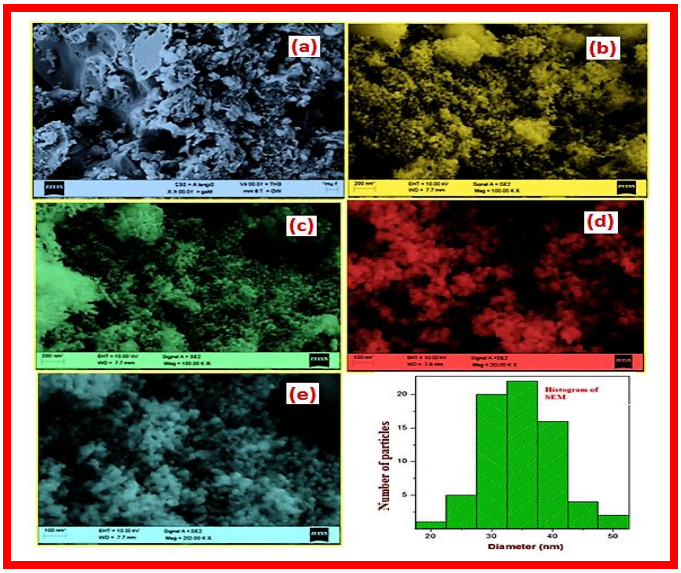

Figure 3 SEM images of (a) undoped (b) 1% (c) 2% (d) 3% (e) 5% Ce^{3+} doped CdO NPs and Histogram of 5% Ce doped CdO

Fig 4 shows EDS spectrum of 5% doped CdO. In the processing option all elements were analysed. The number of iterations was three. The spectrum clearly showed that the elements in the sample were Cd, O and Ce. No other elements were identified in the EDS spectrum. In the sample weight % and atomicity of O, Cd and Ce were found to be 28.34, 54.98, 16.68 and 74.44, 20.55, 5.00 respectively (Table 3).

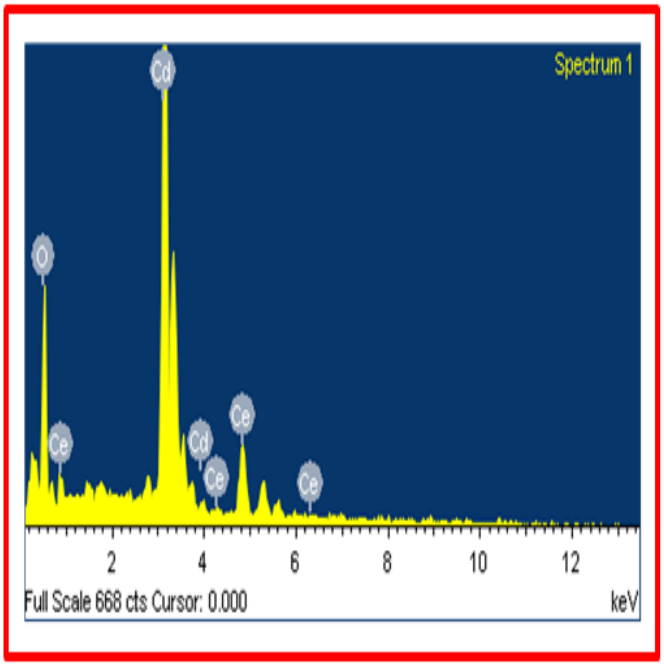

Figure 4 EDS graph of 5% doped CdO

Table 3 EDS report of 5% Ce doped CdO

Element	Weight %	Atomicity %
O K	28.34	74.44
Cd L	54.98	20.55
Ce L	16.68	5
Total	**100**	

The TEM images of 5% doped CdO are shown in Fig 5. The TEM study was carried out to understand the morphology and size of the nanoparticles [20]. The TEM images of doped CdO confirm that the particles are almost spherical with almost uniform thickness. The average particle size by histogram was found to be 50 nm to 200 nm. This image reveals that most of the CdO NPs are spherical in shape and their diameter is about 50 nm. The SAED pattern revealed that the diffraction rings of the synthesized CdO exhibited Debye–Scherrer rings assigned (111), (200), (220), (311) and (222) respectively. The particle size determined from TEM analysis, SEM and XRD were in good agreement.

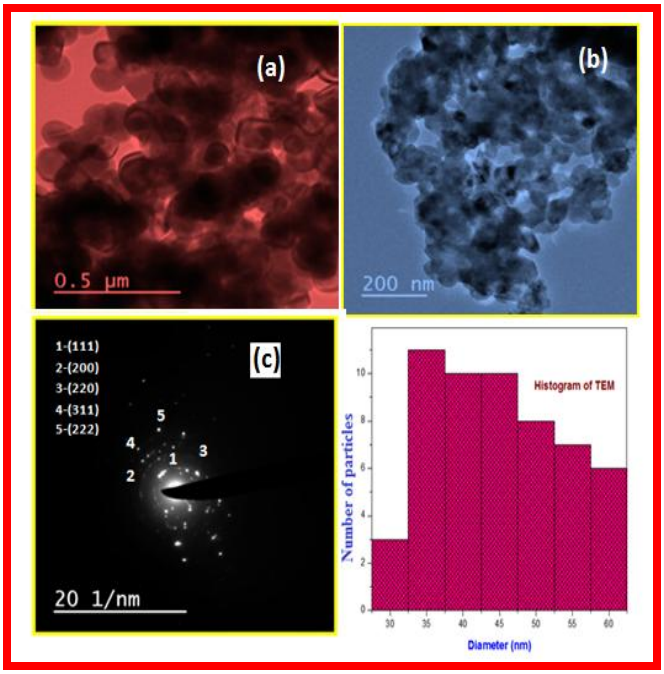

Figure 5 (a) and (b) TEM images of 5% doped CdO and its (c) SAED pattern

2.3 Rietveld refinement

The lattice parameters of all the samples were calculated using Rietveld refinement analysis (Fig 6). The analysis was performed with the FULLPROF software. In order to fit the several parameters to the data point , the function Pseudo–Voigt was used. Two factors (scale, overall B-factor), six cell parameters (a, b, c, α, β and γ),four FWHM parameter (U, V, W and IG), two shape parameter (Etr-0, and X), six background polynomials(a_0 to a_5), four instrumental parameters (Zero, displacement, transparency and wave length) were used for refinement [21]. Table 4 gives lot of information about the refined parameters (atomic functional positions, occupancy). A very good agreement was observed between the simulated intensity (calculated XRD intensities) and experimental relative intensity (observed XRD intensities).

The refined lattice parameters a, b and c were found to be equal and obtained cell volume confirms CdO NPs has a cubic crystal system with Laue class and point group m-3. The goodness of fit (GOF) was found to be 1.4 for Pure CdO which decreases with decrease in particle size. Smaller GOF value confirms good fitting between theoretical plots and experimental plots.

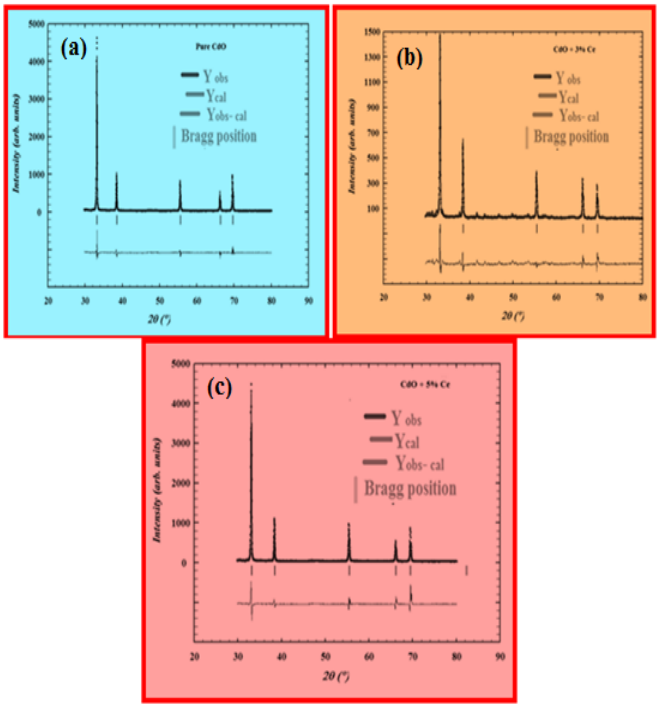

Figure 6 Rietveld refinement of (a) undoped and (b) 3%Ce doped and (c) 5% doped CdO

Table 4 Crystal parameters by Rietveld refinement of undoped and Ce doped CdO

	Pure	0.5%	1%	1.5%	2%	2.5%	3%	5%
Crystal system	**cubic**	**cubic**	**cubic**	**cubic**	**cubic**	**cubic**	**cubic**	**cubic**
Laue class	m-3	m-3	m-3	m-3	m-3	m-3	m-3	m-3
Point group	m-3	m-3	m-3	m-3	m-3	m-3	m-3	m-3
Bravis Lattice	F	F	F	F	F	F	F	F
Lattice symbol	CF	CF	CF	CF	CF	CF	CF	CF
Cell parameters								
a=b=c	4.65	4.66	4.66	4.67	4.67	4.68	4.68	4.69
α=β=γ	90	90	90	90	90	90	90	90
Direct cell volume(A°)^3	101.12	101.7	101.8	102.2	102.2	102.8	102.8	103.1

Atomic coordinates								
Cd								
x	0.72	0.72	0.72	0.72	0.72	0.72	0.73	0.73
y	2.36	2.37	2.37	2.37	2.38	2.38	2.38	2.38
z	2.96	2.96	2.95	2.94	2.94	2.94	2.94	2.94
B	23.01	22.13	19.60	16.06	7.25	4.11	3.37	3.32
occupancy	0.074	0.074	0.075	0.075	0.076	0.075	0.075	0.075
O								
x	1.29	1.30	1.31	1.32	1.32	1.32	1.31	1.34
y	0.71	0.70	0.70	0.70	0.70	0.69	0.72	0.70
z	0.88	0.92	1.0	1.061	1.05	1.07	1.085	1.095
B	15.15	13.52	10.25	7.175	7.148	7.13	2.32	7.137
occupancy	0.046	0.042	0.041	0.0435	0.089	0.143	0.098	0.14
Ce								
x	-	0.55	0.55	0.56	0.56	0.55	0.56	0.55
y	-	0.81	0.81	0.82	0.81	0.81	0.83	0.81
z	-	3.44	3.42	3.46	3.45	1.067	1.063	1.049
B	-	14.32	15.53	16.97	22.33	20.9	16.57	21.02
occupancy	-	0.0017	0.0017	0.0017	0.0017	0.0017	0.0014	0.0017
R_p	14.3	23.5	22.8	21.6	43.9	15	44	18.7
R_{wp}	17.6	31.6	32.9	20.8	33.9	15.8	35.9	18.5
R_{exp}	12.59	24.3	25.6	16.8	27.19	15.1	26.74	16.8
R_{brag}	8.708	7.233	6.375	5.523	3.95	3.67	2.6	2.31
R_F	16.2	15.3	14.59	1.21	2.59	1.86	15.9	10.4
χ^2	1.94	1.32	1.02	1.53	1.56	1.11	1.8	1.21
GOF index	1.4	1.12	1.35	1.2	1.2	1.1	1.3	1.1
Density of compound (g/cc)	182	175	165	155	141	121	121	99

2.4 Packing diagram

The packing diagram for Pure CdO was done using VESTA software which is shown in Fig 7 System of particles was taken to be cubic with space group Fm-3.The lattice parameter a = b = c was chosen to be 4.677 A°. The lattice positions of Cd was (0,0,0) and O was (0.5,0.5,0.5) respectively [22]. From the packing diagram, the bond length between the neighbouring Cd atoms and Cd-O were found to be 3.3128A° and 2.3425A° respectively.

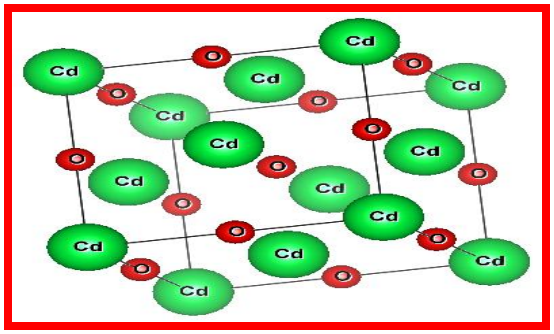

Figure 7 Packing diagram of undoped CdO

2.5 Raman spectroscopy

Fig 8 shows Raman spectra of 5% doped CdO. Pure CdO was found to be Raman inactive [23] but we tried to take the Raman spectrum after doping. Raman measurements on CdO have been reported very rarely. Since CdO structure is similar to that of NaCl, it is expected to have second order Raman spectra. But, non stoichiometric nature of CdO, the O_2 deficiency in the compound destroys the lattice translational symmetry. This will break the selection rules which are based on wave vector conservation. As a result in CdO first and second order spectrum will superimpose showing the perfect crystals weighted density of states. Raman spectra of 5% doped CdO has been measured between 100 cm^{-1} to 1600 cm^{-1}. The observed modes were reconciled with the results of the earlier reports. In addition to smaller peaks major peaks were observed at 251cm^{-1}, 458 cm^{-1}, 855$cm^{-1}$and 900cm^{-1}. Phonon dispersion calculation [24] indicates presence of a transverse optical mode at 251 cm^{-1}, which is a symmetry forbidden presence of disorder which would locally destroy the symmetry and could enable this mode to be observable.

Preliminary Cd K-edge extended X ray absorption spectroscopic studies indicate the presence of both thermal and static disorder. As the highest phonon frequency for CdO reported in is 460 cm^{-1}, the Raman mode at 957 cm^{-1} which corresponds to an overtone. However, even we have got the same modes but slightly shifted that is 458cm^{-1} instead of 460cm^{-1} and 900 cm^{-1} instead of 957 cm^{-1}. This shift was due to the presence of doping element in CdO.

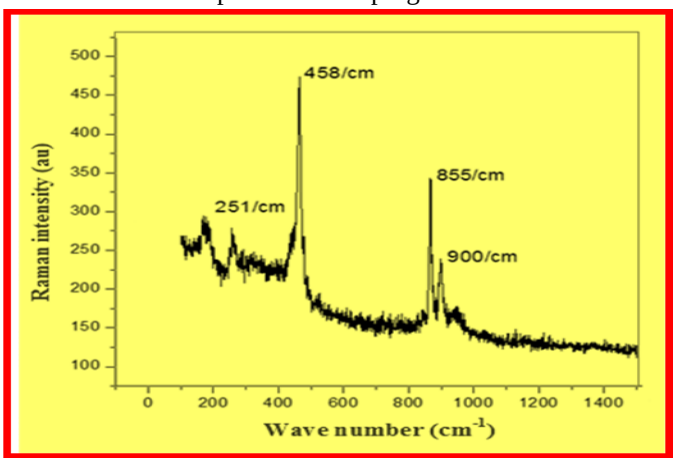

Figure 8 Raman spectra of 5% Ce doped CdO NPs

2.6 Composition studies by XPS

The chemical states and composition of pure CdO and Ce-doped CdO NPs were characterized by XPS. The XPS spectra of CdO and 5% Ce-doped CdO NPs are shown in Fig 9. Two XPS peaks were observed at 405.5eV and 412.54 eV in undoped CdO, which are attributed to Cd $3d_{3/2}$ and Cd $3d_{1/2}$ respectively. After doping these peaks shifts to 413.57 eV and 407.7 eV respectively. Similarly in O, peak was observed at 532 eV in undoped CdO, which is attributed to O 1S and this peak was found to shift to 533.76 eV after doping. Ce peaks attributed to Ce 3d. The shift in the peaks clearly shows that Ce atoms are incorporated into the CdO lattice.

X-ray photoelectron spectroscopy study XPS is one of the strongest techniques which can give qualitative elemental analysis very accurately and quantitative composition with its chemical state (binding and oxidation state). XPS can get information from the top 10 nm surface. XPS is based on the principle of photoelectric effect which was discovered by Hertz in 1887. In XPS X-ray photon with sufficient energy interacts with the solid, which intern eject the electron from its surface. Because of the quantization of energy levels, the distribution of kinetic energy of photo electrons consisting of discrete peaks. These discrete peaks are associated to the electron levels of the photo ionized atom. The emitted electrons have a kinetic energy given by: $E_k = h\nu - E_B - \phi$, where E_k is the kinetic energy of the photoelectrons; $h\nu$, the incident photon energy; E_B , the electron binding energy; and Φ, the work function. E_B can be obtained by measuring E_K. The identification of the elements present on the surface of the sample is directly done by the binding energies of photoelectrons in the core. A typical XPS spectrum is a plot of the Intensity versus the binding energy of the detected photoelectrons.

Deconvolution of XPS of CdO nanoparticles were shown in the Fig 9. Cd components at 406 eV and 413 splitting between Cd $3d_{5/2}$ renders two peaks with binding energies of 405 eV and 407 eV which can be related to $Cd(OH)_2$ and CdO respectively. Similarly peaks at 412 eV and 414 eV at their Cd $3d_{5/2}$ peaks. Moreover two peaks are found for O1s at 531 eV and 533 eV which are due to related CdO systems and are due to the presence of hydroxyl species on the surface.

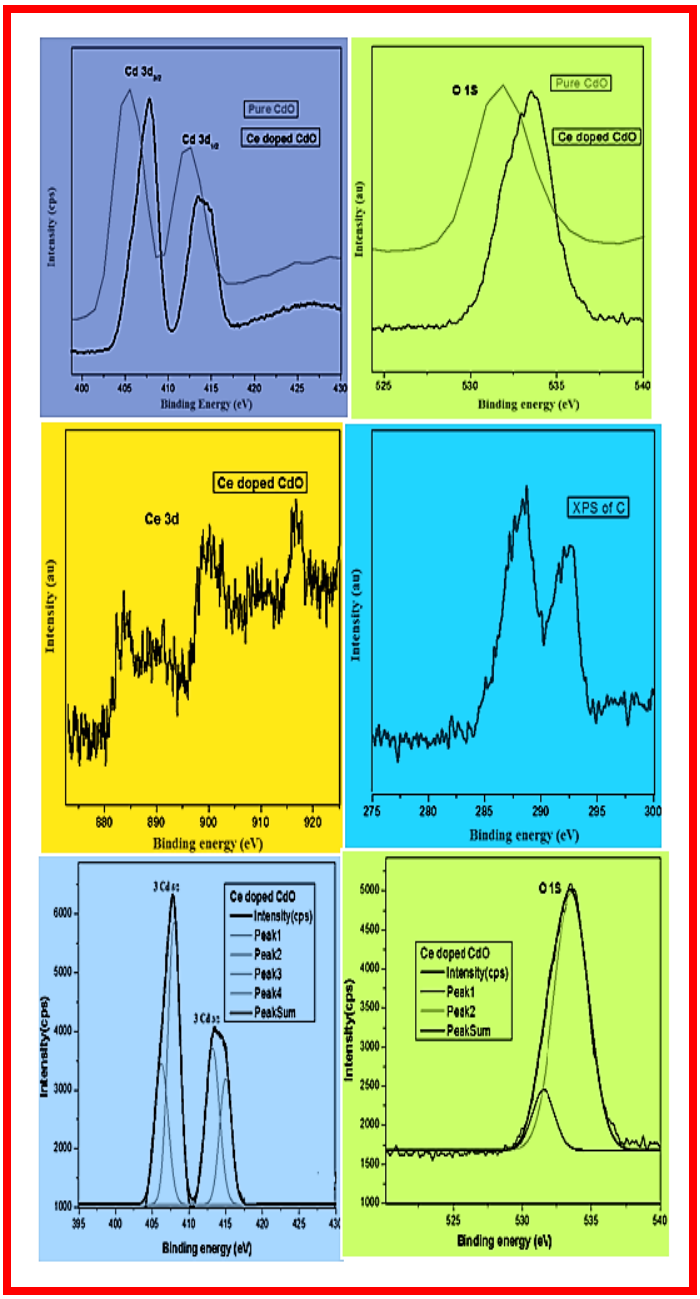

Figure 9 XPS of doped and undoped CdO

2.7 Ferro magnetic studies M-H plot

Fig 10 illustrates the M–H hysteresis loop of 5% Ce doped CdO NPs. For other concentrations the doping percentage was small, we did not get hysteresis loop for them. The readings were taken at room temperature by varying applied field - H(kOe) and corresponding readings of magnetization - M(emu) using vibrating sample magnetometer (VSM). H was applied up to 7 kOe. Clearly the doped sample shows hysteresis (inset) with retentively 0.0109188 emu and coercively 0.008939 kOe. Saturation magnetization was obtained to be 5.2 x 10^{-3} emu. Recently, the same kind of behavior of CdO NPs has been reported by Bououdina et al [25]. The magnetic behavior of metal oxide based NPs such as Al_2O_3 [26] ,CeO_2 [27] , ZnO [28] and SnO_2 [29] at room temperature has been observed and studied by different scientists.. Sundaresan et al. [30] explained that the Ferro magnetic nature of metal oxide NPs may be due to the interaction exchange between localized electron spin moments, which arise due to oxygen vacancy at the surface of metal oxides. He also suggested that all metal oxides may have ferromagnetism as their universal character. This explanation is suitable for the metal oxides which has unpaired spin in its outermost shell. However it is not applicable in our present work.

Electronic configuration of Cd is [Kr] $4d^{10}$ $5s^2$ (Z=48) and O is [He] $2s^2$ $2p^4$ (Z=8). So Cd has completely filled orbits where as O has two unpaired electrons in two of the 2p degenerate orbital. When CdO is formed , then two electrons from Cd can be shared in two ways.

1) Singlet with all the paired electrons in $2p^6$ state of O [total spin zero]

2) Triplet with one unpaired electron in$2p^5$ and one unpaired electron in $3s^1$ orbit [total spin one].

The calculation of structural energy using density functional calculation (DFT) helped us in concluding the feasibility of CdO. Their structural energy for singlet was -123.15 Hartree and that of triplet state was -123.1739 Hartree. Thus structural energy for singlet formation is 0.46 eV more than that of triplet configuration. Thus on the basis of this we can conclude that triplet formation would be the best possible way compared to singlet possibility. This Unpaired electrons in the triplet state may be the explanation for weak ferromagnetic nature of Ce doped CdO NPs at 300K.

2.8 UV-Vis spectroscopy

Fig 11 shows optical absorption spectra of Ce doped CdO NPs. The UV-Vis spectra was taken in the wave length range of 200nm to 600nm. Taking the wave length which corresponds to maximum absorbance in each graph was taken and band gap energy E_g was calculated using the formula $E_g = 1242/\lambda_{max.}$ The wave length corresponded to maximum absorbance for 0.5%, 1%, 1.5%, 2%, 2.5%, 3% and 5% Ce doped CdO and was found to be 412.86 nm,407.03nm, 406.19 nm, 403.74 nm, 402.8 nm, 401.83 nm and 401.39 respectively. The corresponding band gap energy was found to be 3.008 eV, 3.051 eV, 3.0576 eV, 3.076 eV, 3.08 eV, 3.09 eV and 3.094 eV respectively. Thus as particle size decreases, band gap energy increases or the optical absorption spectra of the CdO NPs showed a shift towards blue as compared to bulk CdO. This blue shift was due to the doping and which can be explained by Burstein- Moss effect. Similar kinds of results were observed by other researchers [31].

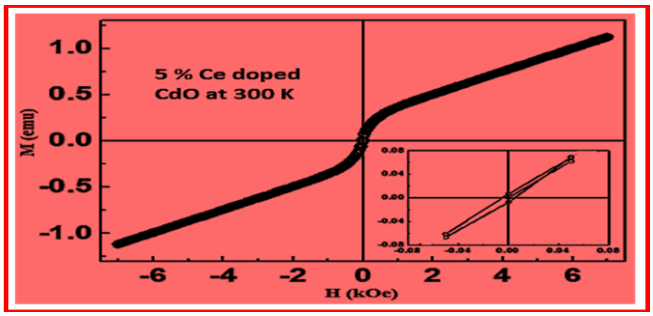

Figure 10 M-H plot 5% Ce doped CdO

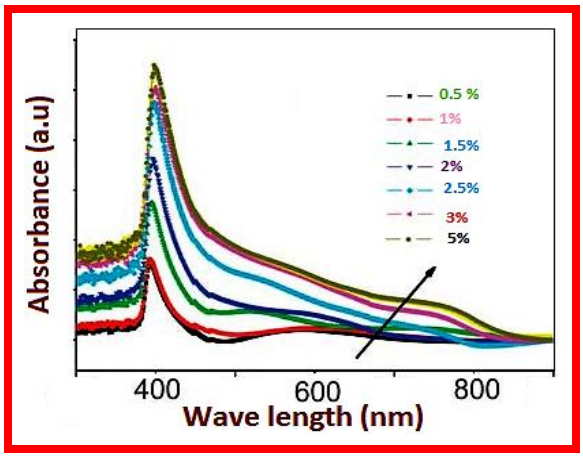

Figure 11 UV-Vis spectra of doped CdO

2.9 Antibacterial activity

Very few researchers have reported the antibacterial activity of doped CdO against human pathogens. Therefore the present investigation reports antibacterial activity of 5% Ce doped CdO on gram positive (*Bacillus subtillis, staphylococcus aureus*) and gram negative (*Escherichia coli, Pseudomonas aeruginosa*) bacteria by disc diffusion method as shown in Fig 12. The present study clearly indicates that the Ce doped CdO NPs can be a very good antibacterial agent both on gram positive and gram negative bacteria.

The diameters of the zone of inhibition were observed for *Bacillus subtillis* and *staphylococcus aureus* were 9mm, 10mm, 14mm, 12mm and 11mm, 10mm, 14mm,12mm respectively. For *Escherichia coli* and *Pseudomonas aeruginosa*, the diameter of zone of inhibition was 11mm, 12mm, 14mm and 16mm, 15mm, 13mm respectively (Table 5). From these results, we can conclude

that Ce doped CdO was more effective on gram positive bacteria than on gram negative bacteria. This may be due to the difference in cell walls of gram positive and gram negative bacteria. Thus Ce doped CdO can be used for cell recovery, DNA synthesis, RNA synthesis and protein synthesis.

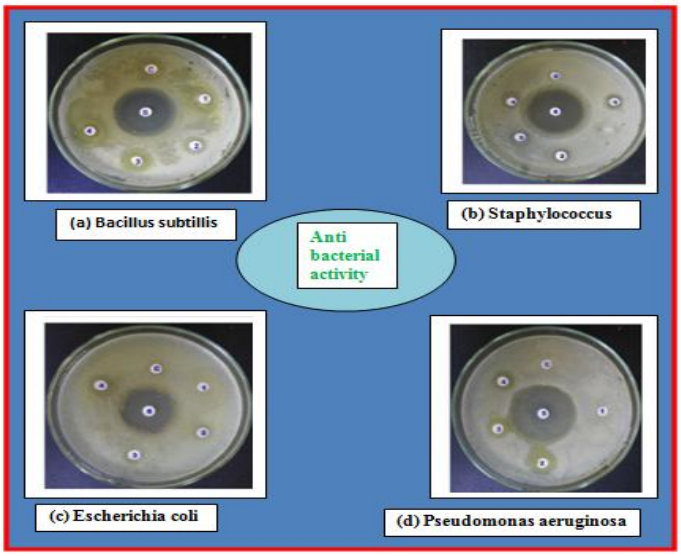

Figure 12 Antibacterial property of 5% Ce doped CdO

Table 5 Anti bacterial activity of 5% Ce doped CdO

Bacteria	Zone of inhibition (mm)			
	A	B	C	D
Bacillus subtillis (Gram positive)	9	10	14	12
Staphylococcus (Gram positive)	11	10	14	12
Escherichia coli (Gram negative)	-	11	12	14
Pseudomonas aeruginosa (Gram negative)	-	16	14	13

3.10 Photoluminescence spectra

A suitable ion is implanted into the solid which is considered as dopant. These dopant ions substitutionally replace the ions of host. The quantity of the dopant ions will be very small compared to host ions. These dopant ions form optically active canters which exhibit the phenomena of photo luminescence, when excited suitably by an appropriate excitation source. The host material plays an important role in determining the nature of optically active dopant ions. This can be explained by crystal field theory or Ligand theory.

Fig. 13(a) shows emission spectra of CdO:Ce^{3+}(0.5 to 5 mol %) nano powders which were excited at 393 nm wavelength. Fig.13b shows the excitation spectrum which was obtained by monitoring the emission centered at 540 nm. The emission spectra of CdO: Ce^{3+} consists of emission peaks at 435nm, 540nm and 646nm and were correspond to Ce^{3+} ion transitions $^5D_3 \rightarrow {}^7F_4$, $^5D_4 \rightarrow {}^7F_5$ and $^5D_4 \rightarrow {}^7F_3$ respectively (Fig 13c). Among the three peaks intense peak was at 435 nm due to $^5D_3 \rightarrow {}^7F_4$ transition. The selection rule for electric dipole (ED) transitions and magnetic dipole transitions are $\Delta J \leq 6$ and $\Delta J=0$ or ± 1 where J is the angular momentum.

The effect of doping Ce^{3+} ions concentration on the intensity of emission spectra of CdO:Ce^{3+} was recorded and is shown in Fig 13(a). Samples with different Ce^{3+} concentration had similar spectra profiles except for 0.5mol% and 5 mol% and no shift peak positions were observed for other Ce^{3+} ions concentration. The PL intensity for all concentrations is the same at 540nm but PL intensity of 0.5 mol% and 5 mol% is more than the other concentration at 435nm where as it is less than that of the other concentration at 646nm.At 435nm PL intensity is maximum and at 646nm PL intensity is small. This can be explained using the concentration quenching effect. At a certain critical value of the doping concentration, the distance between doping ions (Ce^{3+}) becomes small and causes energy migration among Ce^{3+} ions. This brings excitation energy to killer sites which is followed by the quenching effect. It was conventional that the quenching effect due to critical concentration was largely affected by the transfer of energy among Ce^{3+} ions. Thus the critical distance of energy transfer Rc becomes an important factor in explaining concentration quenching effect. As suggested by Blasse [32] , the critical distance of energy transfer Rc was calculated using the $R_c = 2\ [\ 3V/\ 4\pi X_c N\ ]^{1/3}$.

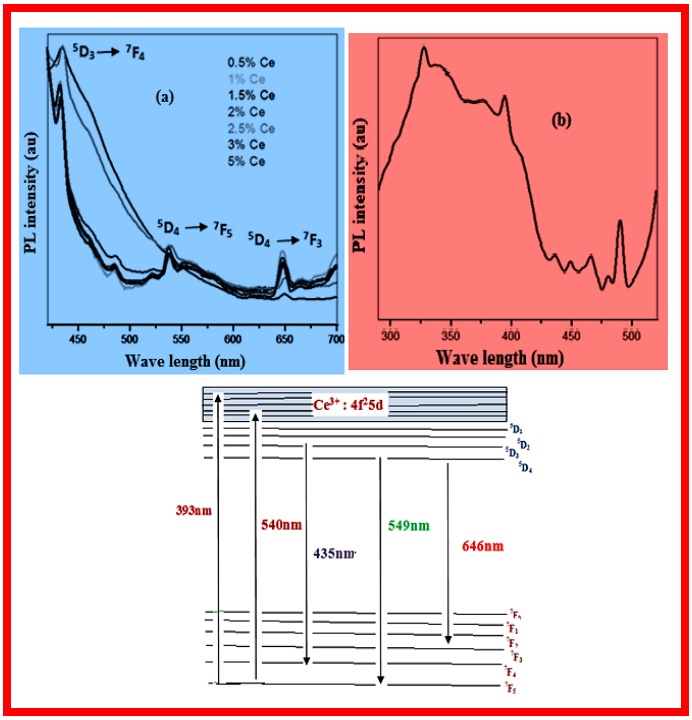

Figure 13 (a) Emission, (b) Excitation spectra and (c) transitions of Ce doped CdO

where unit cell volume is V, number of cations in the unit cell is N and critical concentration X_C. By taking the unit cell volume V as 45.44 $Å^3$, critical concentration as 0.03 and number of cations in the unit cell as 4, we got critical transfer distance as 8.975 Å which is greater than 5 Å. According to the theory of Blasse, exchange interaction becomes ineffective, if the critical transfer distance was greater than 5 Å.. Thus in this case, critical transfer distance is 8.975 Å, exchange interaction becomes ineffective. Thus radiation reabsorption interaction is affected due to the broad overlap of excitation spectrum of the activator and emission spectrum of the sensitizer [32].The equation

$$I/X = k\,[1+\beta(X)^{Q/3}]^{-1} \quad \text{..... (7)}$$

Where *X*; Ce^{3+} ion concentration, k and β; constants, was used to determine the energy transfer between Ce^{3+} ions. According to the above equation log (X) versus log (I/X) will be a linear graph (Fig 14). The slope and intercept of the graph were -1.352 and 5.9201 respectively. The *Q* value is 6 for dipole – dipole interaction, 8 for dipole – quadrupole interaction and 10 for quadrupole – quadrupole interaction. Since the value of *Q* obtained was close to 6, we can conclude the interaction as a dipole dipole interaction[33].

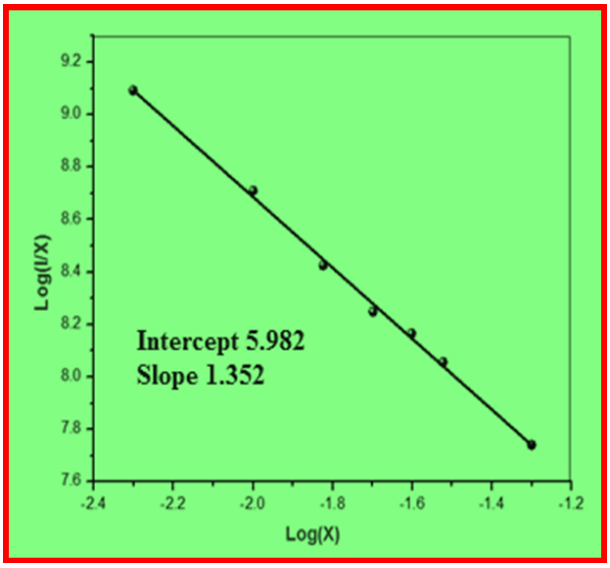

Figure 14 Plot of Log (I/x) Vs Log (x) of CdO:Ce $^{3+}$ nano structures

The Quantum efficiency (Q_E) of CdO: Ce^{3+} (3 mol %) was estimated by the relation $Q_E = [E_c-E_a] / [L_a-L_c]$ ..... (8)

Where E_a: Integral lumen without the sample from the empty integer along sphere

L_a: empty integrating sphere excitation profile

E_c: direct excitation integrated lumen of the phosphor

L_c: Integrated excitation profile when the phosphor was directly emitted by incident photon.

The quantum efficiency was found to be nearly ~ 68.35%.

Colour purities of the obtained sample were also calculated as per the relation.

Color purity =

$$\sqrt{(x_s-x_i)^2+(y_s-y_i)^2}/\sqrt{(x_d-x_i)^2+(y_d-y_i)^2} \quad \text{.....(9)}$$

Where

(x_s, y_s) : Sample point coordinates

(x_d,y_d) : Coordinates corresponding to dominant wavelength and

(x_i,y_i) : highest illumination point coordinates.

The CRI (colour reading index) values were close to 81%. This indicates that the prepared phosphor material was suitable for white light emitting diode related applications.

The emission spectra of rare earth doped host materials was most commonly analysed using the Judd–Ofelt theory [33]. Out of all the transitions the probability of forced electric dipole transition □A_{ed}□ $J \rightarrow J^{l}$□□□was large compared to magnetic dipole transition (*A md*□$J \rightarrow J^{l}$□□. To analyse the transition intensity parameters of Ce $^{3+}$ J-O theory was employed. The chemical environment which affect significantly the luminous properties was studied using J-O theory. For this Ω_t, (t=2,4,6) parameters were determined using emission spectra.

The measured line strengths ($S_{meas}(J \rightarrow J')$) of the selected bands are determined using the following expression:

$$S^{ed}_{meas}(J \rightarrow J') = \frac{3ch(2J+1)}{8\Pi^3 \bar{\lambda} e^2 N_0} \frac{9n}{(n^2+2)^2} \Gamma_{emis} \quad \text{..... (10)}$$

where *J* is the total angular momentum quantum numbers of the initial manifold state and J' is the final manifold states total angular momentum, *c* is the speed of light , *h* is Planck's constant, *n* the refractive index , N_0 is the Ce3+ ion concentration, $\bar{\lambda}$ is the mean wavelength of the specific emission band that corresponds to the $J \rightarrow J'$ transition, $\Gamma = \int \alpha(\lambda)\, d\lambda$ is the integrated absorption coefficient as a function of λ and the factor 9/ $(n^2+2)^2$ is the local field correction for the ion in the dielectric medium.

The Judd-Ofelt theory provides the theoretical expression for the emission line strength $S_{cal}(J \rightarrow J')$ for electric-dipole transitions which is given by

$$S^{ed}_{calc}(J \rightarrow J') = \sum_{t=2,4} \Omega_t \left| \left\langle \varphi^J \left\| U^t \right\| \varphi^{J'} \right\rangle \right|^2$$

..... (11)

where $\left\| U^t \right\|$;the matrix element of rank t (t=2, 4) which is doubly reduced between the terminal and initial states which are characterized by the quantum numbers φ^J and $\varphi^{J'}$ respectively. The least-squares fitting of S_{meas} to S_{calc} provides the two J-O parameters Ω_2 and Ω_4 for Ce^{3+} in CdO host; The

J–O parameters, for various concentrations of Ce^{3+} doped CdO nanophosphors are tabulated in Table 6.

Table 6 Judd-Ofelt intensity parameters (Ω_2, Ω_4), Emission peak wavelengths ($\lambda_p$in nm), radiative transition probability (A_T), calculated radiative (τ_{rad}) lifetime and asymmetric ratio of CdO_3: Ce^{3+} compounds

Ce^{3+} conc. (mol %)	J–O intensity parameters×10^{-20} cm^2		Emission peak wavelength λp(nm)	A_T (s^{-1})	τ_{rad} (ms)	Asymmetric ratio
	Ω_2	Ω_4				
0.5	2.133	1.689	650	187.24	5.19	5.2140
1.0	2.231	1.612	647	185.06	5.33	8.6821
1.5	1.345	1.786	649	144.62	6.81	3.3125
2	0.781	2.112	649	76.72	1.33	2.5314
2.5	0.631	2.236	650	47.57	2.08	2.2416
3	0.412	2.098	648	35.33	2.69	2.1025

In addition to this, some more quantities like the radioative transition rate (A_R), radiative life times (τ_R) and asymmetric was also be determined from the spectra. The radioactive transition rate, radioactive lifetime and asymmetric ratio were calculated using standard procedure [34]. The values of parameter for the Ce^{3+} ion in the CdO host were listed in Table 6. The parameter Ω_2 was related to structural changes in the vicinity of Ce^{3+} ions and covalency. Ω_4 was related to the long-range effect. The obtained values of Ω_2 and Ω_4 were tabulated along with radioactive lifetime in Table 6. Since they all originated from the same excited state, the transition from the individual excited states to the lower-lying manifolds will have the same measured lifetimes. The lattice interactions with the Ce^{3+} ions is the reason for the shorter lifetime for particular transitions.

Commission International de I'Eclairage (CIE) 1931 x-y chromaticity diagram of CdO: Ce^{3+} (1-11 mol %) nanophosphors was shown in Fig 15(a). The corresponding excitation wavelength was 467 nm. The CIE coordinates were located in the Orange region which was in the intersect of Fig 15(a). Correlated colour temperature, CCT was estimated taking the CIE coordinates. CCT was estimated in order to identify the technical applicability of the orange emission. Fig 15(b) gives the CCT diagram of CdO:Ce^{3+} (1 to 11 mol %) nanophosphor. For CdO:Ce^{3+} nanophosphor, the CCTV value was found to be nearly 1720 K. This temperature could be considered as a "cold source of light "[35].

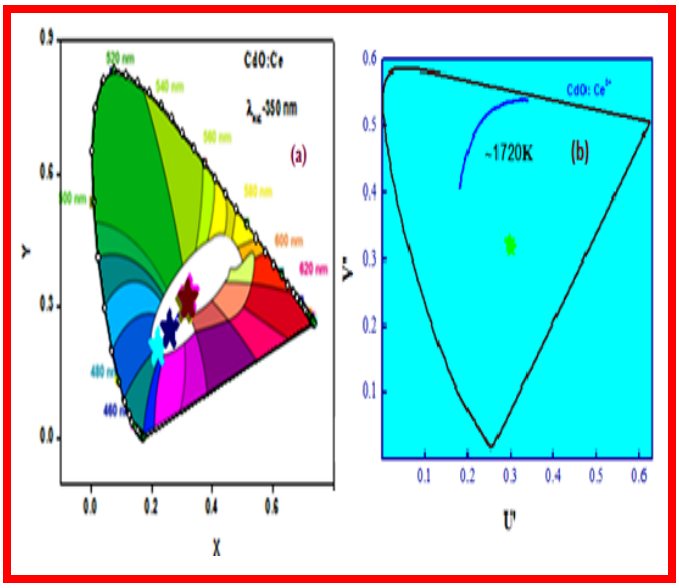

Figure 15 (a) CIE and (b) CCT diagram of CdO: Ce^{3+}

III CONCLUSIONS

For the first time CdO: Ce^{3+} NPs were synthesized and their PL characteristics were studied using J-O theory. CdO NPs with different Ce concentration (0.5 to 5mol%) have been synthesized using combustion method using Aloe vera latex as reducing agent. The morphology of the Ce-doped NPs has been analysed using SEM and TEM techniques. Compositions of the prepared NPs with 5 mol% have been obtained from EDS spectrum. XRD patterns reveals as the doping concentration increases, particle size decreases. Magnified view of (111) shows the peak slightly shifts towards smaller angle which shows that the doping particles are incorporated in the host. Rietveld refinement shows that the particles are having cubic crystal system with lattice symbol CF. The cell parameters a=b=c and α=β=γ were 4.68 A° and 90° respectively. XPS spectra confirmed the presence of Ce as dopant in the sample. Band gap energy increases marginally at 5 mol% due to Burstein-Moss effect. M-H plot shows the material behaves as a weak ferromagnetic substance. Thus Ce doped CdO can be used as wide band gap semiconductors. These wide band gap Semiconductors permit devices to operate at much higher voltages, frequency and temperature than conventional Semiconductors allowing more powerful electrical mechanism to be built which are cheaper and more energy efficient. Thus this can be used in high power application with high breakdown voltage, WLED, Transducers and high electron mobility transistor (HEMT). Since the material is a

ferromagnetic semiconductor, it can be used in spintronics. Its antibacterial characteristic can be used in cell recovery, DNA synthesis, RNA synthesis and protein synthesis.

REFERENCES

[1] Z. Zhao, D.L. Morel, C.S. Ferekides, *Thin Solid Films*, 413(2002)203

[2] Y. Dou, R.G. Egdell, T. Walker, D.S.L. Law, G. Beamson, *Surface Science* 398(1998)241

[3] A.A. Dakhel, *Physics Status Solidi*, 205(2008)2704

[4] R.K. Gupta, K. Ghosh, R. Patel, S.R. Mishra, P.K. Kahol, *Current Applied Physics*, 9(2009)673

[5] A.A. Dakhel, *Thin Solid Films*, 518(2010)1712

[6] P.K.Ghosh, S.Das, K.K.Chattopadhyay, *Journal of Nano Resarch*, 7(2005)219–225

[7] K.S. Kumar, A.Divya, P.S.Reddy, Appllied Surface Science 257(2011)9515–9518

[8] C. Aydın, H.M. El-Nasser, F. Yakuphanoglu, I.S. Yahia, M. Aksoy, *Journal of Alloys Compounds*, 509(2011)854–858

[9] F. Yakuphanoglu, *Solar Energy*, 85(2011)2704–2709

[10] Heshan Zheng, Wanqian Guo, Shuo Li, Renli yin, Qinglian Wu, Xiaochi Feng, Nanqi Ren, Jo-Shu Chang, *Catalysis communications*, 88(2017)68-72

[11] S. Yahia, G.F. Salem, M.S. Abd El-sadek, F. Yakuphanoglu, *Superlattices Microstruct*, 64(2013)178–184

[12] A.A. Dakhel, *Journal of Alloys Compound*, 539(2012)26–31

[13] M. Benhaliliba , C.E.Benouis , A.Tiburcio-Silver , F.Yakuphanoglu , A.Avila-Garcı, A.Tavira, R.R. Trujilloe, Z.Mouffak, *Journal of Luminescence*, 132(2012)2653–2658

[14] T. Aswani, V. Pushpa Manjari, B. Babu, Sk. Muntaz Begum, G. Rama Sundari, K. Ravindranadh, R.V.S.S.N. Ravikumar, *Journal of Molecular Structure*, 1063(2014)178–183

[15] Zayed A. Alahmed, H.A. Albrithen, Ahmed A. Al-Ghamdi, F. Yakuphanoglu, *Optik*, 126(2015)575–577

[16] Sumeet Kumar , SamarLayek, MadhuYashpal, AnimeshK.Ojha, *Journal of Magnetism and Magnetic Materials*, 393(2015)555–561

[17] B. Sahin , Y. Gulen , F. Bayansal , H.A. Cetinkara, H.S. Guder, *Superlattices and Microstructures*, 65(2014)56–63

[18] S. Sivakumar , A. Venkatesan, P. Soundhirarajan, Chandra Prasad Khatiwada, *Spectrochimica Acta Part A: Molecular and Biomolecular Spectroscopy*, 136(2015)1751–1759

[19] S. Sivakumar , A. Venkatesan, P. Soundhirarajan, Chandra Prasad Khatiwada, *Spectrochimica Acta Part A: Molecular and Biomolecular Spectroscopy*, 151(2015)760–772

[20] Lingeshwar sadhasivam, Jenila rani Durai raj, *International journal of chemtech*, 13(2014)4379-4385

[21] H. Ryu, B.K. Singh, K.S. Bartwal, M.G. Brik,*Acta Mate rialia*, 56(2008 358-363

[22] Yendrapati Taraka Prabhu, Kalagadda Venkateswara Rao,Vemula Sesha Sai Kumar,Bandla Siva Kumari ,*World Journal of Nano Science and Engineering*, 4(2014)21-28

[23] Schaack .G and N. Uhle, *solid state communication*, 19(1976)315-318

[24] R.Cusco, J. Ibanez, N. Domenech, Amador,L Artus, J. Zuniga- Perez and V. Munoz sunjose, *Applied physics*, 107(2010)063519

[25] M. Bououdina, A.A.Dakhel, *Alloys and Compound*, 601(2014)162–166

[26] Q. Xu, Z. Wen, H. Zhang, X. Qi, W. Zhong, *Journal of Magnetism and Magnetic Materials*, 393(2015)555–561

[27] S. Phokha, S.Pinitsoontorn, S.Maensiri, *Journal of Applied Physics*, 112(2012)113904-1

[28] G. Yang, D.Gao, J.Zhang, Z.Shi, D.Xue, *Journal of Physics Chemistry C*, 115(2011)16814–16818

[29] C. Wang, M.Ge, J.Z.Jiang, *Applied Physics Letter*, 97(2010)042510-1–042510

[30] A.Sundaresan, R.Bhargavi, N.Rangarajan, U.Siddesh, C.N.R.Rao, *Physical Review Journals B*, 74(2006)161306–161306

[31] Xiaofei Han, Run Liu, Zhude Xu, Weixiang Chen, Yifan Zheng, *Electrochemistry Communications*, 7(2005)1195–1198

[32] G.S. Ofelt, *Jounal of Chemical Physics*, 37(1962)511

[33] Mithlesh Kumar, T.K. Seshagiri, M. Mohapatra, V. Natarajan, S.V. Godbole, *Journal of Luminescence*, 132(2012)2810

[34] C.K. Jorgensen, R. Reisfeld, *Journal of Less Common Metals*, 93(1983)107

[35] S. D. Meetei, S. D. Singh, *Journal of Alloys Compound*, 587(2014)143-147